Chemical Engineering Journal 264 (2015) 1–9

Contents lists available at ScienceDirect

Chemical Engineering Journal

journal homepage: www.elsevier.com/locate/cej

Competitive adsorption of selected non-steroidal anti-inflammatory drugs on activated biochars: Experimental and molecular modeling study

Chanil Jung [a], Linkel K. Boateng [a], Joseph R.V. Flora [a], Jeill Oh [b], Marcus C. Braswell [a], Ahjeong Son [c], Yeomin Yoon [a,*]

[a] Department of Civil and Environmental Engineering, University of South Carolina, Columbia, SC 29208, USA
[b] Department of Civil and Environmental Engineering, Chung-Ang University, 84 Heukseok-ro, Dongjak-gu, Seoul 156-756, South Korea
[c] Department of Environmental Science and Engineering, Ewha Womans University, 52 Ewhayeodae-gil, Seodaemun-gu, Seoul 120-750, South Korea

HIGHLIGHTS

- Biochars prepared in the lab were used to remove NSAIDs.
- Competitive adsorption among NSAIDs was investigated.
- Aromaticity of adsorbent plays a significant role for NSAIDs adsorption.
- Interaction energies between the NSAIDs and the biochar were calculated.

ARTICLE INFO

Article history:
Received 10 October 2014
Received in revised form 14 November 2014
Accepted 15 November 2014
Available online 22 November 2014

Keywords:
Adsorption
Binding energy
Biochar
Diclofenac
Naproxen
Ibuprofen

ABSTRACT

The adsorption of targeted non-steroidal anti-inflammatory drugs: diclofenac (DCF), naproxen (NPX), and ibuprofen (IBP) by two types of activated biochar (N-/O-biochar) was studied in single- and multi-solute adsorption experiments in conjunction with molecular modeling subsequently interpreting the binding energy. The carbonaceous structure of the biochars was elucidated via nuclear magnetic resonance and the intensity of the interactions between the solute and adsorbent was also determined. Using fractions of the carbonaceous functional group on the adsorbent for the single-solute adsorption, the overall binding energies were determined to be in the order of DCF > NPX > IBP ($-21.8 > -17.5 > -14.1$ kcal/mol for N-biochar and $-21.2 > -17.3 > -14.2$ kcal/mol for O-biochar), while the maximum adsorption capacities of DCF, NPX, and IBP for N-biochar and O-biochar were 372, 290, 311 mg/g and 214, 228, 286 mg/g, respectively. A strong interaction between the DCF and the adsorbent resulted in the occupation of effective adsorption sites as compared to other solutes, while blocking the pores in which smaller sized NPX and IBP that may have been adsorbed. A weaker adsorption of IBP was observed in the presence of adsorption competitors. More specifically, the presence of adsorption competitors caused lower binding energy due to a combination of lower binding energy, polarity, and π-energy with the adsorbent and electrostatic repulsion from the cosolutes that occupied adsorption sites.

© 2014 Elsevier B.V. All rights reserved.

1. Introduction

Biochar is a byproduct from the pyrolytic processing of biomass. Its presence significantly improves not only mechanical features of industrial materials, but also chemical properties of soil [1]. It is also plays a critical role in environmental remediation of soil and water by acting as an adsorbent for micropollutants [2]. These potentialities are controlled by feedstock source and pyrolytic profiles (time, temperature, and carrier gas). The carbon and ash content are governed by the feedstock (livestock manure > plant > wood) [3] and the condensed aromatic carbon (400–700 °C) as well as the fraction of functional groups (250–400 °C) are governed by the pyrolysis temperature [4].

Non-steroidal anti-inflammatory drugs (NSAIDs) are often prescribed for the treatment of headaches, arthritis, ankylosing, spondylitis, sports injuries, and menstrual cramps. In fact, they are one of the most prescribed pharmaceuticals. Unfortunately, NSAIDs

---

* Corresponding author. Tel.: +1 (803)777 8952; fax: +1 (803)777 0670.
E-mail address: yoony@cec.sc.edu (Y. Yoon).

http://dx.doi.org/10.1016/j.cej.2014.11.076
1385-8947/© 2014 Elsevier B.V. All rights reserved.

often pass through the patients' digestive system and eventually made their way to water systems via incomplete treatment of human waste. NSAIDs have been detected in trace to considerable levels in the environment [5], and they are known to cause significant renal, degenerative, and necrotic changes on vertebrates [6]. Therefore it is critical to study and understand their fates in order to develop effective treatment and mitigation strategies [7].

Adsorption has been considered as an efficient treatment strategy for organic contaminants in aqueous environment. For instance, Altmann et al. [8] reported the selective and competitive adsorption among carbamazepine, diclofenac, and sulfamethoxazole onto limited surface area of powdered activated carbon, and Sotelo et al. [9] introduced the reduced adsorption ability in the cocktailed solutions of caffeine and diclofenac onto granular activated carbon compared to their single adsorption system, resulting in the reduced adsorption capacity of 29.1% and 32.1%, respectively. The use of carbon nanotubes and activated carbons in this strategy has garnered significant attention due to their high-binding energy and inducement of hydrophobic interaction [10]. Unfortunately, these approaches are insufficient to reveal the adsorption mechanism due to their diversity and intricateness. Therefore, it is required to investigate the additional adsorption mechanisms toward physicochemical properties of both adsorbent and adsorbate. Consideration of the accessibility of the adsorptive sites and pore size of adsorbent in order to minimize the size-exclusion effect and desorption is able to ensure the adsorption mechanism influenced and crucial role in competitive adsorption by characteristics of adsorbent [11].

It is hypothesized that the adsorption of NSAIDs onto activated biochar is related to the binding of NSAIDs onto the surface of the adsorbent at the molecular level. Therefore molecular level simulation of the adsorption process can potentially provide valuable mechanistic insight into the adsorption strength differences between different NSAIDs and various char surface functional groups. Various computational techniques have been employed to study the physisorption of different chemicals onto graphene [12], single-walled carbon nanotubes, and multi-walled carbon nanotubes [13]. However, molecular level studies involving adsorption of chemicals onto biochar has not been explored. This is probably due to the difficulty in generating the exact molecular structure of the char. Previous work by our research group reported the interaction energy associated with the adsorption of atrazine onto hydrochar [14]. In that study, it was found that atrazine was more strongly adsorbed to surfaces without weakly associated alkyl groups.

Xie et al. [15] discovered distinct adsorption ability of demineralized pine wood biochar for sulfamethoxazole and sulfapyridine and reduced adsorption behavior in the presence of humic acid or cation (Cu^{2+}), while Li et al. [16] showed the effect of temperature in sulfamethoxazole adsorption onto the biochar pyrolized at 600 °C. However, there has been less research effort devoted to the biochar under slow and fast pyrolysis produce due to the reverse-proportional relationship between bio-oil production and biochar. Therefore, in this study, the adsorption of three NSAIDs; diclofenac (DCF), naproxen (NPX), and ibuprofen (IBP), onto fast pyrolyzed biochar at 300 °C was investigated to demonstrate the feasibility of simultaneous fulfilment of the effective adsorbent with the bio-oil yield. Physicochemical properties of less carbonized biochars due to low pyrolytic temperature were complemented by chemical activation that increased the surface areas and pore volumes. More specifically we used dispersion-corrected density functional theory in single or competitive adsorptive conditions under consideration of conformation and chemical properties of both solute and adsorbent. Interaction energies between the NSAIDs and the biochar were also calculated to characterize the strength of adsorption and the effect of the various surface functional groups on the adsorption capacity of the char. In addition, each adsorption capacity for both N-biochar and O-biochar was pronounced under single and competitive adsorption systems to evaluate adsorption ability for NSAIDs removal. Throughout the adsorption evaluation, possible adsorption mechanisms were described with molecular modeling.

2. Materials and methods

2.1. Materials

Biochars produced by pyrolyzing torrefied loblolly pine chip (15×6 mm) at 300 °C for 15 min were classified as either N-biochar or O-biochar in terms of pyrolysis with pure nitrogen or 7% oxygen with 93% nitrogen gas, respectively. Both biochars were activated by NaOH to increase the surface area and pore volume of the biochars. The detailed pyrolysis and activation procedures are described in the Supplementary information. Biochars were milled and passed through a 200-mesh (74-μm) sieve, and then stored with ultrapure water (2000 mg/L) for 24 h as a stock solution to hydrate prior to use; the designed dosages of biochar were confirmed by measuring control samples. Three NSAIDs (DCF, NPX, and IBP) and acetonitrile were purchased from Sigma–Aldrich (St. Louis, MO, USA). Their detailed physicochemical properties are provided in the Supporting information (Table S2). A 10 mM stock solution for each NSAID was prepared with acetonitrile solution (anhydrous, 99.8%). The solution was diluted to a target NSAID concentration with ultrapure water after pre-evaporating a known amount of NSAID to minimize any cosolvent effect. Ultrapure water produced by a Milli-Q water filtration system (Millipore, Billeriac, MA, USA) was used for the preparation of all solutions.

2.2. Adsorption experiments

A 20 μM of each pharmaceutical solution was added to 40-mL glass vials equipped with a polytetrafluoroethylene-lined screw cap, and then six known volumes (0.1–0.8 mL) of biochar stock suspension, prepared by adding 200 mg of adsorbent to 100 mL of DI water (2 g/L) and mixing over a magnetic stirrer at 500 rpm, were spiked for the production of a single-solute adsorption isotherm. The pH of the aqueous phase was adjusted to 7 with 1.0 M HCl and NaOH prior to the addition of the adsorbent. Following solute and adsorbent addition, the vials were shaken for 7 d under ambient conditions to achieve equilibrium. After equilibrium, each sample was filtered by 0.22 μm Durapore membrane filters (PVDF) to prevent an adsorption of adsorbates on the filters and concentrations of NSAIDs were analyzed using an Agilent 1200 series high-performance liquid chromatograph (Agilent technologies, Santa Clara, CA, USA). To produce competitive isotherms, bi- and tri-solute adsorption experiments were also performed, and the adsorption method was identical to that used to produce the single-solute isotherm, except for the addition of two or three solutes in the vials. All adsorption experiments were conducted in duplicate or triplicate.

2.3. Characterization of adsorbents

Elemental analysis of the adsorbent was performed on a Perkin-Elmer 2400 Series II CHNS/O Elemental analyzer (PerkinElmer, Waltham, MA, USA). The ash content was determined by heating the biochars to 750 °C and the oxygen content was calculated by subtracting the ash, and carbon, hydrogen and nitrogen contents from the total mass of the samples. Surface and pore characteristics were examined by gas adsorption using a Gemini VII 2390p surface area analyzer (Micromeritics, Norcross, GA, USA). The total pore volume was calculated from the adsorbed quantity of N_2 at $P/P_0 = 0.95$, and the surface area was determined by the Brunaer–Emmett–Teller (BET) equation with multipoint adsorption isotherms of N_2 at 77 K. Solid-state ^{13}C DP/MAS (direct polarization/magic angle spinning) nuclear magnetic resonance (NMR) spectra were acquired using a 3.2-mm MAS probe on a Varian Inova 500 spectrometer (Palo Alto, CA, USA). The ^{13}C NMR spectra combined with dipolar-recoupled NMR methods were used for quantitative structural analyses of the biochars. The detailed experimental conditions used for the NMR experiments are described elsewhere [17].

2.4. Molecular modeling for solutes and adsorbents

The initial structures for seven representative biochar configurations were generated in Gaussview based on NMR surface functional group measurements and char structures proposed in the literature [18]. The geometries of the biochar structures and NSAIDs were optimized using dispersion-corrected density functional theory [19] with the BLYP functional, and the 6-31++G(d,p) basis set in TeraChem [20]. The initial configurations for the biochar–NSAID complexes (BIO-DCF, BIO-NPX and BIO-IBP) were obtained by optimizing fragments of the biochar–NSAID complexes by following the geometry optimization procedures described in a previous study [21]. Competitive adsorption of the different NSAIDs onto the biochar surfaces was simulated by randomly locating the center of a competing NSAID molecule between 1.5 and 5 Å from the center of a fixed BIO-NSAID complex. A total of 10,000 optimized configurations were collected and the lowest-energy configurations that were representative of competitive adsorption were selected for further geometry optimization at the DFT-D/BLYP/6-31++G(d,p) level. Aqueous phase adsorption energies were calculated using the SMD continuum solvation model implemented in GAMESS [22]. Final solvated energy calculations for the complexes were performed at the DFT-D/BLYP/6-31++G(d,p) level, and the binding energies (ΔE) between the biochar and the NSAIDs were calculated as:

$$\Delta E = E(\mathrm{BIO} + \mathrm{NSAID}) - E(\mathrm{BIO}) - E(\mathrm{NSAID})$$

In the case of competitive adsorption, the binding energies between the biochar and the competing NSAIDs were calculated as:

$$\Delta E_C = E\left(\mathrm{BIO} + \mathrm{NSAID}^1 + \mathrm{NSAID}^2\right) - E\left(\mathrm{BIO} + \mathrm{NSAID}^1\right) - E\left(\mathrm{NSAID}^2\right)$$

where ΔE_C is the binding energy (kcal/mol) between the biochar and the NSAID^2 in the presence of a competitor NSAID^1. Binding energies between the NSAIDs and N-biochar and O-biochar were approximated based on the NMR surface functional group measurements.

3. Results and discussion

3.1. Characterization of biochars

The ^{13}C NMR spectra and elemental composition of two different precursor biochars were markedly different. A quantitative spectral analysis for ^{13}C DP/MAS NMR revealed that both aromatic and aryl carbon (108–148 ppm) were dominant in N-biochar and O-biochar, while N-biochar was composed of higher aliphatic carbon; alkyl (0–45 ppm), methoxyl (45–63 ppm), carbohydrate (63–108 ppm), and carboxyl carbons (165–187 ppm). This indicated that N-biochar had a higher surface polarity than O-biochar, whereas O-biochar contained more aromatic carbon than N-biochar, with higher peak values (Table 1 and Fig. S1). More condensed aromatic carbon, as indicated by the higher fraction of non-protonated carbon in O-biochar than in N-biochar, was analyzed by the ^{13}C DP/MAS and dipolar dephasing experiments (Table S3). The increased aromaticity of O-biochar resulted from the supplemental combustion between alkyl carbons and oxygen, which produced additional heat in the pyrolysis process [23]. A higher pyrolysis temperature produced a higher carbon content, an aromatic carbon fraction with a more condensed cluster, and a higher surface area, while it produced a lower biochar yield, and low oxygen and ash contents [4]. The 7% oxygen in pyrolysis induced the increase in final temperature, and resulted in expanding the structure with larger size of biochar and greater ash content at even lower oxidation levels [24]. The presence of oxygen in the pyrolysis for biochar production with the activation caused more fixed carbon than the activated N-biochar, which was pyrolyzed under pure nitrogen-purged system, and more detailed values about the proximate analyses of biomass and biochars are described in Table S1.

In contrast, fully charred N-biochar allowed an enhancement of oxygen during activation, with a higher polarity on the surface of the material itself due to the accessible activated layers [25]. The examination of the pore structure of the biochars identified a reasonably large surface area and pore volume. More disordered structures provide more open and closed sectors on the biochar [26]. An adsorption facilitative open sector allows interaction with molecules in solution [11], and it was assumed that N-biochar, with twice as much macro-pore volume compared to O-biochar, would achieve a higher level of adsorption in this study. The more condensed aromatic carbon cluster in O-biochar mitigated the effect of chemical activation, resulting in less effective porous structural properties.

3.2. Interaction energy

Hydrophobic interactions and π–π electron donor–acceptor (EDA) interactions were considered to evaluate the mechanisms in the interactions between activated biochar and NSAIDs. Based on the interaction configuration, the binding energy was calculated as a function of Van der Walls and electrostatics. Figs. S2 and S3 show the optimized configurations of the biochar–NSAID complexes. DCF interacted more favorably than NPX and IBP with the biochar structures as a result of its larger molecular butterfly structure, which maximizes π–π interactions between the surface of the biochar and the solute, resulting in high binding energy [27]. In its lowest energy configuration, DCF interacted with the biochar structures at a minimum distance of 3.5 Å, with one aromatic ring oriented parallel to the surface of the biochar and the other perpendicular to the adsorbent surface. The simulation results were consistent with the experimental observations, where a higher fraction of DCF was adsorbed onto the biochar.

Interactions between biochar and NPX were more favorable than for IBP with one methyl group directed toward the surface of the adsorbents, although the carbohydrate functional group on the biochar was an exception with the carboxyl group of NPX oriented away from the biochar surface with a minimum intermolecular distance of 3.5 Å (Fig. S2). The smaller molecular structure of IBP resulted in reduced π–π interactions and dispersion forces between the solute and adsorbent due to less surface area exposure to the biochar surface, which resulted in an overall reduction in the binding energies. Single-solute adsorption experiments however indicated preferential adsorption of IBP onto biochar, compared to DCF and NPX. This could be attributed to the higher dependence of IBP adsorption on a hydrophobicity effect, which was not fully captured in the simulations. The gas phase and implicit SMD simulations estimated binding energies on the basis of

Table 1
Properties of activated biochars.

Samples	C (%)	H (%)	N (%)	O (%)	H/C	Polarity index		Ash (%)	SA-N_2 (m^2/g)	Pore volume (cm^3/g)	
						N/C	O/C			Micro-pore	Macro-pore
Elemental composition, aromatic ratio, ash content, BET-N_2 surface area (SA-N_2), and cumulative pore volume of biochars											
N-biochar	72.6	0.77	0.65	21.3	0.127	0.001	0.221	4.7	1360	0.307	0.643
O-biochar	83.8	0.24	0.30	13.0	0.034	0.003	0.116	2.7	1151	0.313	0.318
Samples	Aliphatic C (%)			Aromatic C (%)		Carbonyls (%)		Aliphatic C (%)	Aromatic C (%)	Aromaticity (%)[a]	Polar C (%)[b]
	Alkyl 0–45 ppm	Methoxyl 45–63 ppm	Carbohydrate 63–108 ppm	Aryl 108–148 ppm	O-aryl 148–165 ppm	Carboxyl 165–187 ppm	Carbonyl 187–220 ppm				
Quantitative spectral analysis for solid-state ^{13}C DP/MAS NMR for biochars (calculated based on 100% carbon in each biomass)											
N-biochar	7.14	4.81	21.5	45.7	9.91	8.22	2.79	33.5	55.6	62.5	47.2
O-biochar	2.80	2.42	18.5	57.8	10.1	5.07	3.32	23.7	67.9	74.1	39.4

[a] Aromaticity = aromatic C (108–165 ppm)/[aliphatic C (0–108 ppm) + aromatic C (108–165 ppm)].
[b] Total polar carbon = (45–108 ppm) + (148–220 ppm); Table was modified from Jung et al. [29].

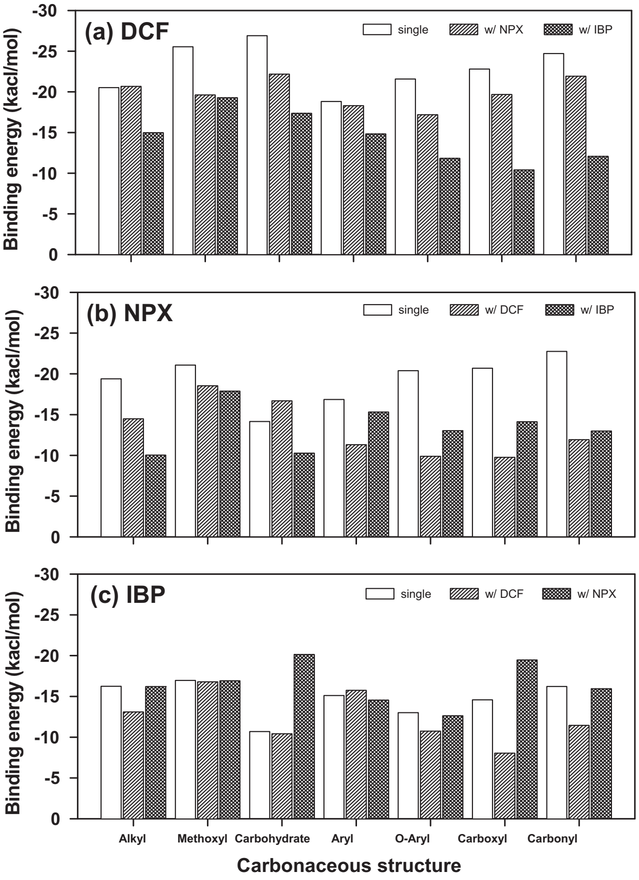

(a.1) DCF overall binding energy (kcal/mol)

Competitor	N-biochar	O-biochar
None	-21.8	-21.2
NPX	-19.5	-19.2
IBP	-14.9	-14.8

(b.1) NPX overall binding energy (kcal/mol)

Competitor	N-biochar	O-biochar
None	-17.5	-17.3
DCF	-12.8	-12.4
IBP	-13.6	-13.9

(c.1) IBP overall binding energy (kcal/mol)

Competitor	N-biochar	O-biochar
None	-14.1	-14.2
DCF	-13.2	-13.7
NPX	-16.2	-15.8

Fig. 1. Binding energy distribution of (a) DCF, (b) NPX, and (c) IBP with respective to carbonaceous structure base analyzed by NMR and overall binding energies (a.1, b.1, and c.1) in the condition of non-competitive and competitive adsorption.

available molecular surface area and did not fully account for the hydrophobicity effect on the adsorption process.

The interaction energies associated with the binding of the NSAIDs onto N-biochar and O-biochar were estimated based on the percentage of carbon in each functional group. The results together with the energy contribution from the individual functional groups are presented in Fig. 1 and Tables S4 and S5. Overall, the NSAIDs interacted more favorably with N-biochar than O-biochar despite the high aromaticity value of O-biochar. The high interaction strength of the NSAIDs with N-biochar can be attributed to its high BET-N_2 surface area, which has an overall greater impact on the adsorption capacity than the aromatic carbon fraction in the functional groups. A significant energy contribution from the aryl and carbohydrate functional groups was observed in both N-biochar and O-biochar. This was apparently due to the high percentages of the functional groups in both types of biochar, which affected the overall binding energies between solute and adsorbent.

The interaction strength of DCF and NPX decreased during competitive adsorption in the presence of other NSAIDs. For a given adsorption site, the presence of a competing solute may lead to a reduction in the available adsorption sites that are accessible to the main NSAIDs. In the simulations, this translated to a reduction in the accessible adsorbent surface area, which resulted in an overall reduction in the interaction strength between the main NSAIDs and the adsorbent. The interaction strength of DCF with N-biochar decreased by 6.9 and 2.3 kcal/mol in the presence of IBP and NPX competitors, respectively. For O-biochar, reductions of 6.4 and 2.0 kcal/mol were observed. Similarly, the interactions of NPX with the adsorbents were mitigated by reduction of binding energy of 3.9 and 4.7 kcal/mol for N-biochar and 3.4 and 4.9 kcal/mol for O-biochar in the presence of IBP and DCF as a competitor, respectively. However, the interaction of IBP with N-biochar and O-biochar increased by 2.1 and 1.6 kcal/mol, respectively, in the presence of NPX as a competitor; while the presence of DCF reduced the overall binding energy between biochars and IBP.

3.3. Single-solute adsorption

The Langmuir adsorption model was applied to adsorption data in this work, due mainly to the comparison between experimental results and monolayer adsorption-based molecular modeling rather than multilayer adsorption-based model, Freundlich isotherm (Fig. S4). The model has the following linear form:

$$\frac{C_e}{q} = \frac{C_e}{q_{max}} + \frac{1}{K_L q_{max}} \qquad (1)$$

where C_e is the solute equilibrium concentration (mg/L) in the aqueous phase; q is the mass of adsorbed solute on a unit mass of adsorbent (mg/g); q_{max} is the maximum mass adsorbed at the saturated adsorption capacity of adsorbent (mg/g); and K_L is the empirical constant (L/mg).

Adsorption isotherms on N- and O-biochars are displayed for NSAIDs in Fig. 2. Although the adsorption affinity of NSAIDs onto the biochar determined by molecular modeling followed the order of DCF > NPX > IBP, the experimental adsorption results differed slightly from those of molecular modeling due to limited consideration of open sectors on the biochar and the physicochemical properties of both the solute and adsorbent (Table 2).

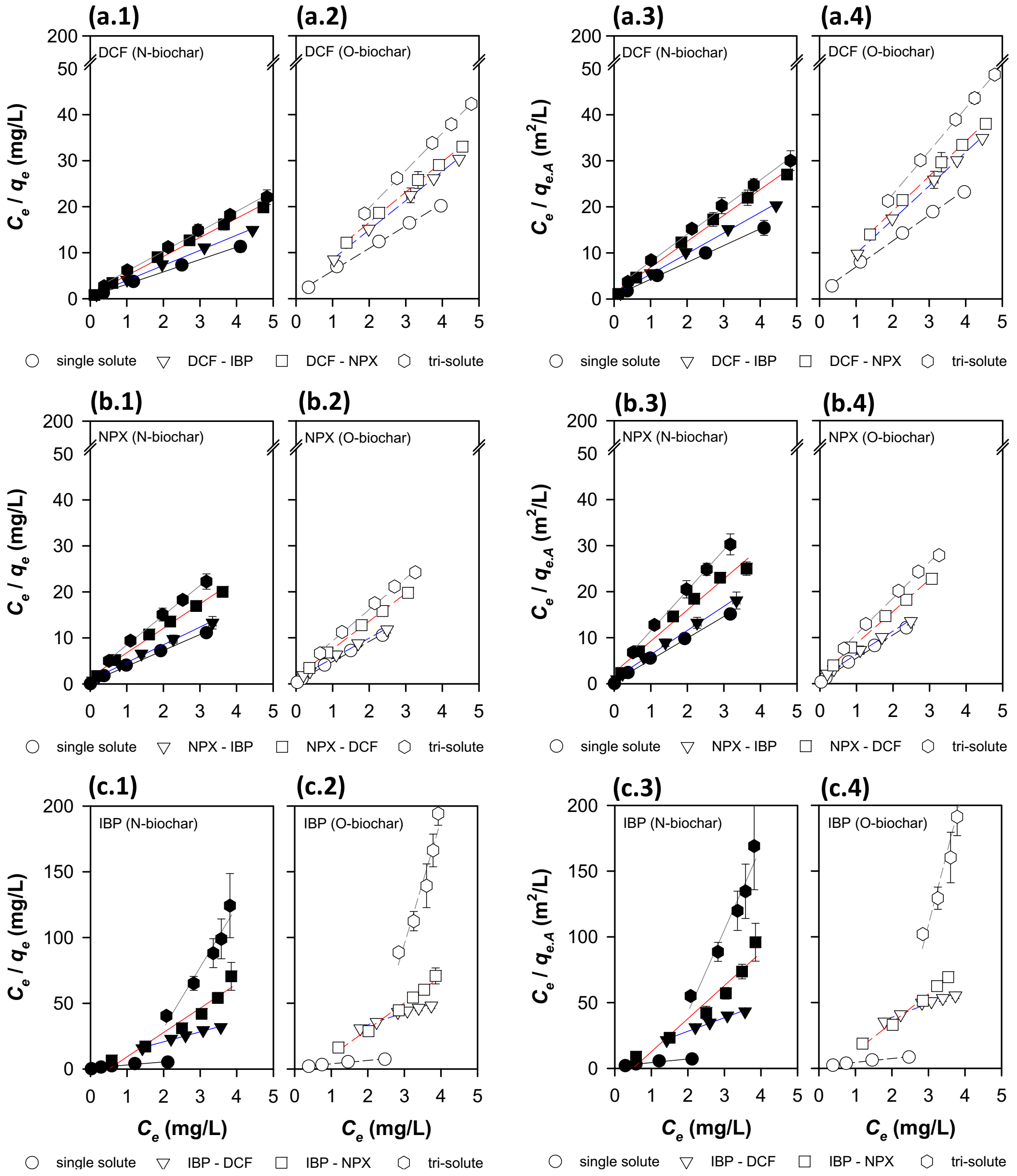

Fig. 2. Langmuir model data fitting for NSAIDs by N-biochar (black) and O-biochar (white) in the condition of single-solute (circle), bi-solute (triangle and square), and tri-solute system (hexagon) (C_0 = 20 μM).

Table 2
Langmuir isotherm parameters for adsorption of NSAIDs on biochars (mass).

Competitor	DCF				NPX				IBP			
	Single	Double		Triple	Single	Double		Triple	Single	Double		Triple
	–	IBP	NPX	All	–	IBP	DCF	All	–	DCF	NPX	All
N-biochar												
$q_{\max}$	372	305	242	231	290	243	178	155	311	132	62.6	25.3
K_L	5.89	4.80	4.59	2.67	8.90	6.59	4.85	3.20	8.02	1.35	−3.02	−0.903
R^2	0.990	0.996	0.993	0.990	0.994	0.992	0.994	0.990	0.983	0.986	0.965	0.929
O-biochar												
$q_{\max}$	214	161	155	124	228	213	166	147	286	109	52.6	14.6
K_L	3.19	2.46	1.73	2.25	10.9	5.07	3.95	2.70	6.81	0.601	−2.40	−0.635
R^2	0.994	0.997	0.995	0.998	0.997	0.995	0.998	0.996	0.991	0.940	0.986	0.910

Unit of q_{max}: (mg/g); K_L: (L/mg).

3.3.1. Diclofenac adsorption

DCF adsorption behavior differed between N- and O-biochars, with a maximum adsorption capacity of 372 and 214 mg/g, respectively. A strong interaction between aromatic carbon on the biochar and DCF was dominant due to the π–π EDA interaction between polar aromatic DCF (electron acceptors) and the polarizable biochars (electron donors) [28]. Relatively large size of DCF molecules appeared to be an important factor for DCF adsorption. For the micro-sized pores in the open sector it was assumed that a sieving effect occurred in DCF adsorption. The greater number of large sized pores on N-biochar allowed better contact with DCF, resulting in considerable adsorption differences to smaller pore-sized other carbonaceous adsorbents [29]. This sieving effect was identified by surface area normalized isotherms (Fig. 2 and Table S6). The area normalized maximum adsorption capacity values for DCF indicated that N-biochar was a superior adsorbent with respect to DCF adsorption than O-biochar. Despite the higher aromaticity and binding energy with DCF of the O-biochar, the contribution of the polarity of N-biochar increased the adsorption affinity of DCF [30] due to the relatively high molecular polarizability and π-energy values of DCF compared to NPX and IBP. Regardless of the elemental composition and the ratio of carbonaceous structure, the binding energy between each structure and DCF was estimated to be above −20 kcal/mol, except for that between aryl carbon and DCF (−18.8 kcal/mol). Although non-aromatic carbon, aliphatic carbon, and carbonyls had higher binding energies with DCF, the small fraction of non-aromatic carbon did not play a critical role in DCF adsorption, while aromatic carbon did encourage the hydrophobic interaction due to the component ratio.

3.3.2. Naproxen adsorption

NPX adsorption behavior on N- and O-biochars displayed a similar tendency to DCF adsorption, with maximum adsorption capacities of 290 and 228 mg/g, respectively. The maximum adsorption capacity ratio of O-biochar to N-biochar was 0.79, and this value was higher than the ratio for DCF (0.57) (Table S6). This distinctive NPX adsorption capacity of each biochar was dissipated with surface area normalization, with only 7% difference, due to the smaller size of the NPX molecule, less influenced sieving effect, compared to DCF. NPX was able to occupy both open and closed sectors with no hindrances. The lower adsorption capacity of NPX than DCF was due to the lower hydrophobicity. Due to the relatively low K_{ow} and pK_a values of NPX, the hydrophobicity expressed was lower than 1 in log D, resulting in a lesser overall binding energy compared to DCF. However, naphthalene-based aromatic structures of NPX employed not only strong π–π EDA interaction but also high Van der Waals force with the biochars, and improved the adsorption behaviors such as an adsorption strength and capacity (Table 2) [31].

3.3.3. Ibuprofen adsorption

IBP was estimated from the molecular modeling to be the least favorable solute for adsorption onto biochars. The adsorption experiments, however, indicated preferential adsorption of IBP onto the biochars compared to DCF and NPX. This discrepancy could be attributed to the higher dependence of IBP adsorption on not only the hydrophobicity effect, which was not fully captured in the simulations, but also its smaller molecular structure, which enabled it to occupy more small sites on the exposed surface area of the biochar [32]. The relatively higher hydrophobicity (log $D_{ow} = 1.82$ at pH = 7) led to the binding energy deficiency derived from the single benzene ring structure to be overcome, and the small molecular dimensions were considered to be sufficient for adsorption onto the small sized pores in the open sector of the biochars. This strong hydrophobic interaction was explained by surface area nominalization at the maximum adsorption capacity. Macro-sized pores in N-biochar were regarded as a closed sector for IBP, and mitigated the sieving effect due to the small size of IBP, resulting in a ratio of the surface area normalized maximum adsorption capacity of O-biochar to that of N-biochar of 1.09 (Table S6). This excess led to magnification of the hydrophobic interactions in IBP adsorption.

Another factor affecting the evaluation of IBP adsorption is partitioning. A partitioning coefficient is usually calculated by means of dual-mode sorption in a single-solute system [33], and its effect is correlated with the conformation and polarity of an adsorbent for the removal of organic pollutants (naphthalene, nitrobenzene, and m-dinitrobenzene) that is dominated by a monolayer surface cover [34]. However, the conformation of both biochars was only marginally correlated to the partition of NSAIDs (Table S7 and Fig. S5). The partitioning of NSAIDs was inversely proportional to molecular polarity for O-biochar due to its lower polarity and higher aromatic carbon content [35]. These hydrophobic interaction favored properties may interrupt the partitioning, which was evident in the inverse relation between the adsorptive role of hydrophobic interaction and the partitioning. The lower polarity of IBP promoted partitioning along with total adsorption, and this adsorption mechanism was attributed to the partition between trichloroethene and other low polarity compounds, and soil organic matter [36]. Therefore, this weak binding between the low-polarity IBP and the polar section of the biochars could describe partitioning and total sorption, while the lower polarity was negligible in terms of controlling the adsorption behavior.

3.4. Bi-solute adsorption

To compare competitive effect of individual cosolutes with the adsorption of each NSAID onto the biochars, the competitive adsorption between DCF vs. NPX, NPX vs. IBP, and IBP vs. DCF is plotted in Fig. 2. The maximum adsorption capacity was compared to that in the single adsorption system and is listed in Table 2 and S6.

Competition of cosolutes with DCF on both biochars followed the order at the same thermodynamic state: NPX > IBP. The DCF maximum adsorption capacities on N- and O-biochars were 18% and 25%, respectively, in the presence of IBP, and 35% and 27%, respectively, in the presence of NPX compared to the value of its single adsorption capacity. Because a given adsorbent has limited sorption sites, the higher binding energy between DCF and the biochars contributed to the occupation of the closed sector on the adsorbents and hindered hydrophobic interactions between IBP and the biochars [37]. This cloud effect of the occupied DCF provided less opportunity for interaction between IBP and the aromatic fraction of the biochars, and the degree of this hindrance was greater for O-biochar due to its higher aromaticity compared to N-biochar. This shield of adsorption sites was a consequence of the strong interaction between the larger projected area of DCF and adsorption sites on the adsorbent, and IBP was more affected due to its smaller cross-sectional area with a lower binding energy. Moreover, the larger molecular size of DCF blocked the micropores, which were occupied preferentially by the smaller IBP molecules. The adsorption capacity of IBP then decreased sharply in the presence of DCF, with 58% and 62% reductions observed on N- and O-biochars, respectively. The higher hydrophobicity did not prevent the reduction in adsorption due to the lower binding energy and pore blockage in the competitive adsorption system, and similar results were obtained [38].

The similar cosolute effects for NPX to DCF and DCF to NPX adsorption were examined due to their analogous dominant adsorption mechanisms; i.e., hydrophobic interactions such as π–π EDA interactions and polar interactions, which resulted in adsorption capacity of N-biochar and O-biochar as 35% and 27% in the presence of IBP, 38% and 27% in the presence of DCF, respectively, compared to the value of its single adsorption capacity. The greater hydrophobic interactions and higher polarity and π-energy of DCF indicated its considerable adsorption affinity toward the aromatic fraction of the adsorbent, resulting in the same tendency for the overall single-solute system.

A cosolute effect was observed between IBP and NPX; that is, IBP appeared to disrupt the adsorption of NPX. Compared to the adsorption capacity of NPX in the single-solute system, 84% and 93% of NPX were adsorbed onto the N- and O-biochars, respectively. The NPX also prevented IBP from occupying adsorption sites on the adsorbent, with only 20% and 18% of the IBP adsorbed onto N- and O-biochars, respectively, compared to the adsorption capacity of IBP in the single-solute system. The relatively weak binding energy between IBP and the biochars was increased dramatically in the presence of NPX as a cosolute, while the binding energy between NPX and the biochars was reduced, resulting in a lower overall binding energy in the competitive adsorption with IBP (Fig. 1). Although a steep increase in the binding energy between IBP, and carbohydrate and carboxyl carbon on the adsorbent led to this energy reverse phenomenon, these non-aromatic interactions acted as a disruptor of other aromatic interactions, with a repulsive effect that mitigated the hydrophobic interaction [39]. Therefore, the theoretical overall binding energy between IBP and biochars was higher than that for NPX. The lower binding energy between IBP and aromatic adsorbents enabled the adsorption sites to have greater affinity toward NPX on the aromatic sites, and this phenomenon was more marked with O-biochar due to its higher proportion of aryl and O-aryl fractions.

Another distinguishable feature of the cosolute effect was the enhancement of π-cloud overlap or π–π interaction due to the planar steric NPX, naphthalene (two benzene rings)-based structure, with the adsorbent [40]. This planarity effect was reliable in terms of the comparison between similar molecular sized compounds, and was verified by the additional driving force (π–π interaction) between planar solutes (phenanthrene, benzo(a)anthracene) and graphene structured char rather than a compound containing one benzene ring (phenol, 2,2-methyllene-bis) with nonspecific Van der Waals interactions [38]. Hydrogen containing functional groups on the biochar, increased the number of competitive deprotonated IBP and NPX in neutral water conditions (neutral pH), acting as a H-donor and H-acceptor, presumably, leading to the small proportion of hydrogen bonding. The adsorption by hydrogen bonding was more pronounced between IBP and biochar due to relatively high hydrogen favorable property, and higher value of binding energy between hydrogen containing functional groups and IBP supported this distinction (Fig. 1(c)). Moreover, the higher polarity of NPX enhanced its affinity toward the adsorbent when excess water was present due to the partial deionization of the molecules at pH 7, with higher p*Ka* values [38]. Unlike the competitive adsorption with DCF, the pore-blockage effect between the similar sized IBP and NPX molecules was negligible.

3.5. Tri-solute adsorption

The representation of tri-solute competitive adsorption was convoluted by the energy difference due to the complexity in configuration during the molecular modeling. However, the typical and dominant adsorption mechanisms in single- and bi-solute systems were considered to interpret the tri-solute system. The unchangeable physical properties of adsorbent for tri-solute adsorption played a crucial role to reveal the mechanisms rather than chemical reactions (binding energy, hydrophobic interaction, etc.). In contrast to the significant increase in the multi-solute adsorption predicted by Polanyi theory based on micro-pore filling without considering the flat surface adsorption [41], the total amount of adsorbed solutes in the tri-solute system was increased

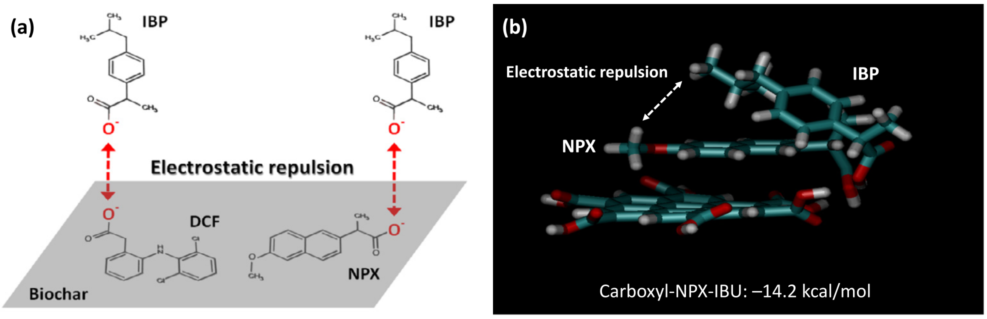

Fig. 3. Schematics of (a) electrostatic repulsion between protonated IBP and DCF and/or NPX in the competitive adsorption on the biochar, and (b) optimum condition of competitive adsorption of NPX in the presence of IBP in terms of binding energy model data fitting with carboxyl based biochar.

slightly compared to the single- and bi-solute systems (Table 2). In the concept of monolayer adsorption, rather than multi-layer adsorption approach with a low concentration of each solute ($C_e/C_s < 1$), was ascribed to the relatively large surface area and pore volume of the biochars compared to other carbonaceous adsorbents. The adsorptions in the tri-solute system were similar but slightly lower than that of bi-solute system for both DCF or NPX, resulting in the range of adsorption capacities of as 53–65% of each single-solute system value, whereas adsorption for IBP in the tri-solute system achieved only 8% and 5% of the adsorption capacity of the single-solute system with N- and O-biochars, respectively. This was attributed to its lower competitive adsorption affinity. IBP in the tri-solute system was deprived of adsorption sites because they were occupied by DCF and NPX due to their higher binding energy with the adsorbent, higher polarity, and larger molecular size. The precarious and weaker affinity features of IBP toward the biochars in the presence of adsorptive competitors was caused by a repulsive effect between deprotonated IBP and the negatively charged adsorbent surfaces due to the occupation of deprotonated DCF and NPX (Fig. 3) [42].

4. Conclusions

Various analyses were undertaken to better understand each property of the solutes and adsorbent and evaluate their adsorption affinity and capacity, respectively. In particular, the characterization of biochars via NMR analysis has allowed the evaluation of their structure and properties, while molecular modeling has revealed the intensity of binding energy between adsorption media. Molecular modeling of solutes and adsorbents has enhanced our understanding of binding energy with consideration of both the conformation and polarity of adsorbents and the physicochemical properties of NSAIDs. This new method enabled the investigation of specific hydrophobic interactions, which are dominant in the pharmaceutical adsorption system. Distinct adsorption ability of N-biochar than that of O-biochar was caused by the carbonaceous structure, which was formed in a pyrolytic condition under pure nitrogen carrier gas. To perform more accurate and reliable interpretations, further studies should apply not only multi-layer adsorption but also consider a number of cases of competitive adsorption under various water matrices. Finally, the fundamental fate of selected micro-pollutants and an understanding of the adsorption system on biochars will contribute to not only the improvement of the removal efficiency of adsorbents, but also prevent exposure to harmful chemicals under more complex environmental conditions.

Acknowledgements

This research was financially supported by the Korea Ministry of Environment, 'Project, 414-111-006'. This study was also partially supported by the University of South Carolina ASPIRE and STEM programs.

Appendix A. Supplementary data

Supplementary data associated with this article can be found, in the online version, at http://dx.doi.org/10.1016/j.cej.2014.11.076.

References

[1] J. Lehmann, J. Gaunt, M. Rondon, Bio-char sequestration in terrestrial ecosystems–a review, Mitig. Adapt. Strat. Gl. 11 (2006) 395–419.
[2] J. Ni, J.J. Pignatello, B. Xing, Adsorption of aromatic carboxylate ions to black carbon (biochar) is accompanied by proton exchange with water, Environ. Sci. Technol. 45 (2011) 9240–9248.
[3] J.M. Novak, I. Lima, B. Xing, J.W. Gaskin, C. Steiner, K. Das, M. Ahmedna, D. Rehrah, D.W. Watts, W.J. Busscher, Characterization of designer biochar produced at different temperatures and their effects on a loamy sand, Ann. Environ. Sci. 3 (2009) 2.
[4] B. Chen, D. Zhou, L. Zhu, Transitional adsorption and partition of nonpolar and polar aromatic contaminants by biochars of pine needles with different pyrolytic temperatures, Environ. Sci. Technol. 42 (2008) 5137–5143.
[5] M.J. Benotti, R.A. Trenholm, B.J. Vanderford, J.C. Holady, B.D. Stanford, S.A. Snyder, Pharmaceuticals and endocrine disrupting compounds in US drinking water, Environ. Sci. Technol. 43 (2008) 597–603.
[6] J. Treadgold, Q.-T. Liu, J.A. Plant, N. Voulvoulis, Pharmaceuticals and personal-care products, Pollutants, Human Health and the Environment: A Risk Based Approach (2012) 207.
[7] J.L. Packer, J.J. Werner, D.E. Latch, K. McNeill, W.A. Arnold, Photochemical fate of pharmaceuticals in the environment: naproxen, diclofenac, clofibric acid, and ibuprofen, Aquat. Sci. 65 (2003) 342–351.
[8] J. Altmann, A.S. Ruhl, F. Zietzschmann, M. Jekel, Direct comparison of ozonation and adsorption onto powdered activated carbon for micropollutant removal in advanced wastewater treatment, Water Res. 55 (2014) 185–193.
[9] J.L. Sotelo, G. Ovejero, A. Rodríguez, S. Álvarez, J. Galán, J. García, Competitive adsorption studies of caffeine and diclofenac aqueous solutions by activated carbon, Chem. Eng. J. 240 (2014) 443–453.
[10] D.S. Salloum, J.B. Schlenoff, Protein adsorption modalities on polyelectrolyte multilayers, Biomacromolecules 5 (2004) 1089–1096.
[11] K. Yang, X. Wang, L. Zhu, B. Xing, Competitive sorption of pyrene, phenanthrene, and naphthalene on multiwalled carbon nanotubes, Environ. Sci. Technol. 40 (2006) 5804–5810.
[12] D. Cortés-Arriagada, L. Sanhueza, M. Santander-Nelli, Modeling the physisorption of bisphenol A on graphene and graphene oxide, J. Mol. Model. 19 (2013) 3569–3580.
[13] L.K. Boateng, J. Heo, R.V.J. Flora, Y.-G. Park, Y. Yoon, Molecular level simulation of the adsorption of bisphenol A and 17α-ethinyl estradiol onto carbon nanomaterials, Sep. Purif. Technol. 116 (2013) 471–478.
[14] J.F.R. Flora, X. Lu, L. Li, J.R.V. Flora, N.D. Berge, The effects of alkalinity and acidity of process water and hydrochar washing on the adsorption of atrazine on hydrothermally produced hydrochar, Chemosphere 93 (2013) 1989–1996.
[15] M. Xie, W. Chen, Z. Xu, S. Zheng, D. Zhu, Adsorption of sulfonamides to demineralized pine wood biochars prepared under different thermochemical conditions, Environ. Pollut. 186 (2014) 187–194.
[16] T. Li, X. Han, C. Liang, M. Shohag, X. Yang, Sorption of sulphamethoxazole by the biochars derived from rice straw and alligator flag, Environ. Technol. (2014) 1–9.
[17] J. Park, J. Meng, K.H. Lim, O.J. Rojas, S. Park, Transformation of lignocellulosic biomass during torrefaction, J. Anal. Appl. Pyrol. 100 (2013) 199–206.
[18] X. Cao, K.S. Ro, M. Chappell, Y. Li, J. Mao, Chemical structures of swinemanure chars produced under different carbonization conditions investigated by advanced solid-state ^{13}C nuclear magnetic resonance (NMR) spectroscopy, Energy Fuel. 25 (2011) 388–397.
[19] S. Grimme, S. Ehrlich, L. Goerigk, Effect of the damping function in dispersion corrected density functional theory, J. Comput. Chem. 32 (2011) 1456–1465.
[20] J. Kastner, J.M. Carr, T.W. Keal, W. Thiel, A. Wander, P. Sherwood, DL-FIND: an open-source geometry optimizer for atomistic simulations, J. Phys. Chem. A 113 (2009) 11856–11865.
[21] Q. Zaib, I.A. Khan, N.B. Saleh, J.R. Flora, Y.-G. Park, Y. Yoon, Removal of bisphenol A and 17β-estradiol by single-walled carbon nanotubes in aqueous solution: adsorption and molecular modeling, Water Air Soil Pollut. 223 (2012) 3281–3293.
[22] A.V. Marenich, C.J. Cramer, D.G. Truhlar, Universal solvation model based on solute electron density and on a continuum model of the solvent defined by the bulk dielectric constant and atomic surface tensions, J. Phys. Chem. B 113 (2009) 6378–6396.
[23] R.F. Drnevich, G.W. Fenner, H. Kobayashi, L.E. Bool III, Production enhancement for a reactor, Google Patents, 2006.
[24] M.X. Fang, D.K. Shen, Y.X. Li, C.J. Yu, Z.Y. Luo, K.F. Cen, Kinetic study on pyrolysis and combustion of wood under different oxygen concentrations by using TG-FTIR analysis, J. Anal. Appl. Pyrol. 77 (2006) 22–27.
[25] P. Vinke, M. Van der Eijk, M. Verbree, A. Voskamp, H. Van Bekkum, Modification of the surfaces of a gas activated carbon and a chemically activated carbon with nitric acid, hypochlorite, and ammonia, Carbon 32 (1994) 675–686.
[26] W.J. Braida, J.J. Pignatello, Y. Lu, P.I. Ravikovitch, A.V. Neimark, B. Xing, Sorption hysteresis of benzene in charcoal particles, Environ. Sci. Technol. 37 (2003) 409–417.
[27] J.R. Schames, R.H. Henchman, J.S. Siegel, C.A. Sotriffer, H. Ni, J.A. McCammon, Discovery of a novel binding trench in HIV integrase, J. Med. Chem. 47 (2004) 1879–1881.
[28] W. Chen, L. Duan, D. Zhu, Adsorption of polar and nonpolar organic chemicals to carbon nanotubes, Environ. Sci. Technol. 41 (2007) 8295–8300.
[29] C. Jung, J. Park, K.H. Lim, S. Park, J. Heo, N. Her, J. Oh, S. Yun, Y. Yoon, Adsorption of selected endocrine disrupting compounds and pharmaceuticals on activated biochars, J. Hazard. Mater. 263 (2013) 702–710.
[30] P. Küsgens, M. Rose, I. Senkovska, H. Fröde, A. Henschel, S. Siegle, S. Kaskel, Characterization of metal–organic frameworks by water adsorption, Microporous Mesoporous Mater. 120 (2009) 325–330.

[31] S.D. Chakarova-Käck, E. Schröder, B.I. Lundqvist, D.C. Langreth, Application of van der Waals density functional to an extended system: adsorption of benzene and naphthalene on graphite, Phys. Rev. Lett. 96 (2006) 146107.

[32] W. Xu, Q. Gao, Y. Xu, D. Wu, Y. Sun, W. Shen, F. Deng, Controllable release of ibuprofen from size-adjustable and surface hydrophobic mesoporous silica spheres, Powder Technol. 191 (2009) 13–20.

[33] E. Graber, A. Sorek, L. Tsechansky, N. Atzmon, Competitive uptake of trichloroethene and 1, 1, 1-trichloroethane by *Eucalyptus camaldulensis* seedlings and wood, Environ. Sci. Technol. 41 (2007) 6704–6710.

[34] Z. Chen, B. Chen, D. Zhou, W. Chen, Bisolute sorption and thermodynamic behavior of organic pollutants to biomass-derived biochars at two pyrolytic temperatures, Environ. Sci. Technol. 46 (2012) 12476–12483.

[35] B.L. Sawhney, K.W. Brown, Reactions and movement of organic chemicals in soils, Soil Sci. Soc. Am. (1989).

[36] B. Xing, J.J. Pignatello, B. Gigliotti, Competitive sorption between atrazine and other organic compounds in soils and model sorbents, Environ. Sci. Technol. 30 (1996) 2432–2440.

[37] X. Ren, C. Chen, M. Nagatsu, X. Wang, Carbon nanotubes as adsorbents in environmental pollution management: a review, Chem. Eng. J. 170 (2011) 395–410.

[38] M. Sander, J.J. Pignatello, Characterization of charcoal adsorption sites for aromatic compounds: insights drawn from single-solute and bi-solute competitive experiments, Environ. Sci. Technol. 39 (2005) 1606–1615.

[39] M. Miah, Z. Iqbal, E.P. Lai, Rapid CE-UV evaluation of polypyrrole-coated magnetic nanoparticles for selective binding of endocrine disrupting compounds and pharmaceuticals by aromatic interactions, Anal. Methods 4 (2012) 2866–2878.

[40] T.D. Bucheli, Ö. Gustafsson, Quantification of the soot-water distribution coefficient of PAHs provides mechanistic basis for enhanced sorption observations, Environ. Sci. Technol. 34 (2000) 5144–5151.

[41] M. Manes, Activated carbon adsorption fundamentals, Encyclopedia of environmental analysis and remediation 1 (1998) 26–68.

[42] V. Yangali-Quintanilla, A. Sadmani, M. McConville, M. Kennedy, G. Amy, Rejection of pharmaceutically active compounds and endocrine disrupting compounds by clean and fouled nanofiltration membranes, Water Res. 43 (2009) 2349–2362.